Ramirez Hoyos, P.; Cervera, J.; Nasir, S.; Mubarak, A.; Ensinger, W.; Mafe, S. (2023). Electrochemical impedance spectroscopy of membranes with nanofluidic conical pores. Journal of Colloid and Interface Science. 655:876-885. https://doi.org/10.1016/j.jcis.2023.11.060

Electrochemical impedance spectroscopy of membranes with nanofluidic conical pores

Patricio Ramirez,[a,*] Javier Cervera,[b] Saima Nasir,[c,d] Mubarak Ali,[c,d] Wolfgang Ensinger,[d] Salvador Mafe[a,b]

[a]*Departament de Física Aplicada, Universitat Politècnica de València, E-46022 València (Spain)*
[b]*Departament de Física de la Terra i Termodinàmica, Universitat de València, E-46100 Burjassot (Spain)*
[c]*Materials Research Department, GSI Helmholtzzentrum für Schwerionenforschung, D-64291 Darmstadt, Germany*
[d]*Department of Material- and Geo-Sciences, Technische Universität Darmstadt, D-64287 Darmstadt (Germany)*

Electrochemical impedance spectroscopy (EIS) constitutes a useful tool in membrane science and technology because it provides valuable structural and functional information. The different arcs observed in the impedance spectra permit to decouple and understand distinct physico-chemical phenomena occurring under operating conditions. By using EIS techniques, we have characterized here multipore asymmetric membranes with conical pores that exhibit a broad range of ionic conduction properties, including current rectification. These properties can be modulated by tuning the electrical interaction between the charges functionalized on the pore surface and the nanoconfined ionic solution. In particular, the membrane electrical response is studied as a function of the amplitude and frequency of the external voltage signal, the electrolyte type and concentration, and the solution pH. Remarkably, significant chemical inductance effects are observed. The scalability and biocompatibility of these pores suggest good potential for use in hybrid biodevices and interfaces.

---

*Corresponding author. E-mail address: patraho@fis.upv.es

Keywords: Membrane characterization, Nanofluidic conical pores, Electrochemical impedance spectroscopy, Chemical inductances

1. Introduction

The surface-regulated ionic conduction of nanopores is usually studied by using direct currents. However, alternating current (AC) techniques are useful to analyze frequency-dependent capacitance and inductance effects. Equivalent circuit models can reveal the system geometric factors and surface properties, together with the dynamic ionic transport processes, through the impedance loops observed in different frequency ranges [1-16]. Hysteresis and memory processes are central to the frequency-dependent functionality of electronic and electrochemical pore-based devices [17-24].

Electrochemical impedance spectroscopy (EIS) constitutes a useful tool to characterize and optimize porous materials such as nanotubes, nanosheets, and membranes [1-10] in contemporary science and technology. EIS can provide valuable structural and functional information concerning micro and nanoscale interfacial processes such as fouling, water splitting, and biosensing [1-6,8,9,11-13,15], both in surface and bulk phases. The different arcs observed in the impedance spectra permit to decouple and understand the distinct physico-chemical phenomena occurring simultaneously in complex electrochemical systems under operating conditions.

Nanofluidic iontronics is largely based on surface chemistry concepts, being central to modern membrane applications in electrochemical energy transducers, logical circuits in sensing and actuating, and signal processing in bioelectrical interfaces [4,17,22-24]. By using EIS techniques, we have characterized here multipore membranes with nanoscale conical pores that display a broad range of ionic conduction properties, including current rectification. These properties arise from the electrical interaction between the charges functionalized on the pore surface and the nanoconfined ionic solution [25-28]. Thus, the basic concepts involved can also be relevant to bioelectrochemical systems [17,18,22,23,29].

The nanoporous membrane characteristics are described as a function of the amplitude and frequency of the external voltage signal, the electrolyte type and concentration, and the solution pH. The scalability and biocompatibility of the pores also suggest great potential for hybrid biodevices and interfaces based on the simple operational functions and their reliability with respect to the case of single-nanopores [17,18,20-22,29].

2. Experimental

Figs. 1a–d show the experimental setup and the electrochemical cell, together with the current (I) – voltage (V) and dV/dI–V curves, of the nanoporous membrane with conical pores. The cell was confined in a double–layer magnetic shield (Amuneal, Philadelphia) and placed on an anti–vibration table (Technical Manufacturing Corporation, Peabody, Massachusetts) [29,30]. The membranes were 12.5 μm thick polyimide foils (Kapton50 HN, DuPont) irradiated at *UNILAC* linear accelerator (GSI, Darmstadt) with swift heavy Au ions [31,32]. Asymmetric track–etching procedures were used to convert the ion tracks into conical pores whose carboxylate residues gave surface charge densities between –0.1 and –1.0 e/nm^2 at neutral pH, where e is the elementary charge [30-32]. On the basis of the SEM images of pore fractures together with electrical conductance measurements, typical pore radii were found in the ranges 10 – 40 nm (cone tip) and 300 – 800 nm (cone base) [30]. The exposed membrane area was ca. 1 cm^2 and contained typically 200 – 300 pores.

Currents and voltages were monitored by Ag|AgCl electrodes equipped with 2M KCl salt solution bridges connected to a potentiostat (BioLogic SP–200, Seyssinet–Pariset, France). The left solution bathed the pore tip while the right solution bathed the pore base. LiCl 99% NaCl 99.5%, KCl 99.5% and $CaCl_2$ 99.0% salts were purchased from PanReac AppliChem (FRG) and ITW Reagents (Italy) and used as received. Before and after each measurement, the pH solution values and the ambient temperature (295 K) were controlled. The asymmetric

multipore membrane showed low conductances at voltage $V < 0$, which corresponds to the current entering the cone base in Fig. 1b, and high conductances at $V > 0$, which corresponds to the current entering the cone tip (Fig. 1c) [25].

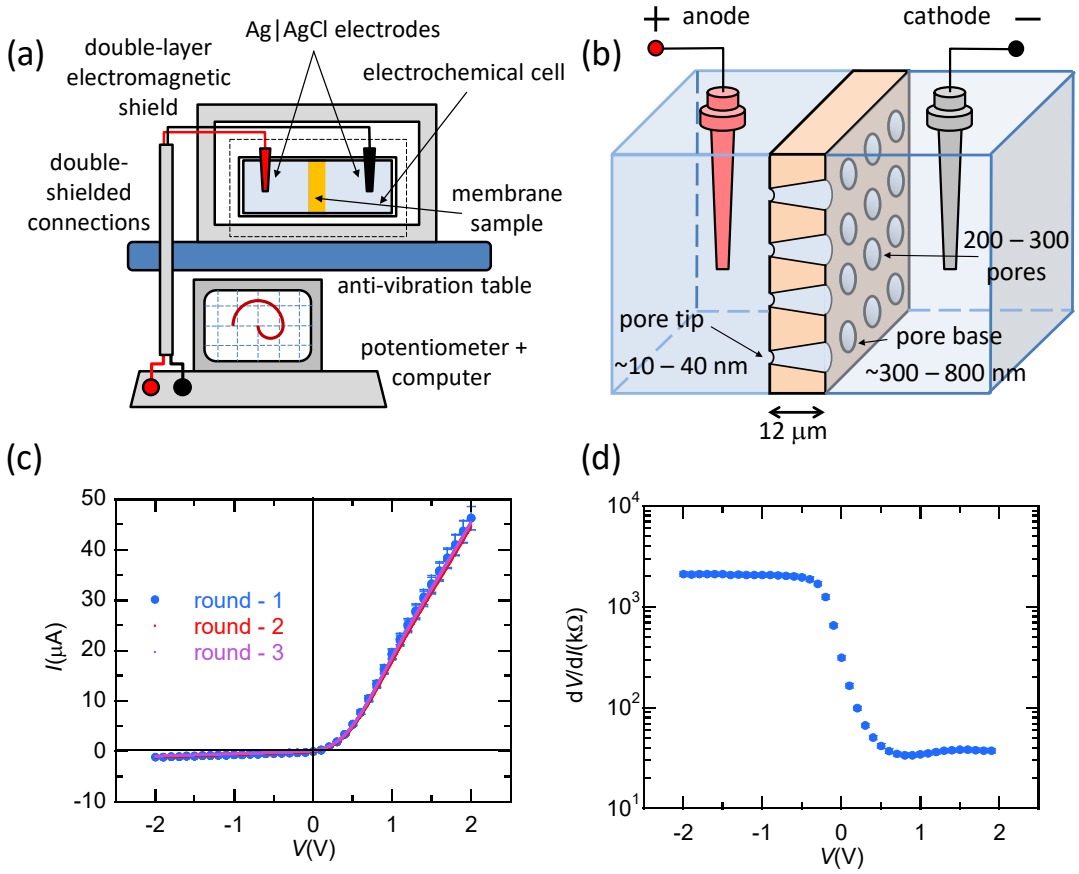

Fig. 1 (a) Scheme of the experimental setup. The electrochemical cell is connected to the potentiostat, located within a magnetic shield, and mounted on an anti–vibration table. (b) Detail of the experimental cell with the multipore membrane and the Ag/AgCl electrodes. (c) Typical current (I)–voltage (V) curves obtained with a 100 mM KCl solution at neutral pH for membrane sample #1. The curves were measured during three independent experimental runs with the picoammeter–voltage source (Keithley 6487, Keithley Instruments), round 1, and the potentiostat, rounds 2 and 3 (BioLogic SP–200). Two independent measurements obtained with the potentiostat voltage source together with one measurement obtained with a are shown. The experimental errors remained below 5%. (d) The corresponding differential resistance dV/dI *vs.* voltage V curve. Note that the error bar lengths are similar to the experimental point sizes.

The uncertainties of Fig. 1c arise from the time variability of the samples along different experimental runs. During one-month period, different measurements were carried out to check both the current-voltage curves and the impedance spectra at 100 mM KCl and different conditions. All over the measurement period, the experimental errors remained below 5% for the current-voltage curves (see Figure 1 where two different protocols were used on three different days) and below 10% for the impedance spectra at $V = -0.5$ V, 0 V, and 0.5 V (see Figure 2). Note also that the limits of the $I - V$ curve at high positive and negative voltages give constant values of the differential resistance (Fig. 1d), as expected.

3. Results and discussion

Fig. 2 shows the real (Re) and imaginary (Im) components of the membrane impedance Z as a function of the voltage signal frequency f, together with the Nyquist plot Im (Z) *vs.* Re(Z), for negative (Figs. 2a – c), zero (Figs. 2d – f), and positive (Figs. 2g – i) voltage V amplitudes. Note that Re(Z) tends to the differential resistance dV/dI when the frequency f tends to zero, thus providing reliable estimations of the membrane ionic resistance. As it could be expected from the $I - V$ curves (Figure 1c), the impedances are higher for reverse ($V < 0$) than for forward ($V > 0$) polarization. Interestingly, a maximum in the Re(Z) curve (Fig. 2g), together with chemical inductance [33] effects characterized by $-\mathrm{Im}(Z) < 0$ (Figs. 2h and 2i), are evident at $V > 0$. These effects are not observed for reverse (Figs. 2b and 2c) and zero (Figs. 2e and 2f) polarizations.

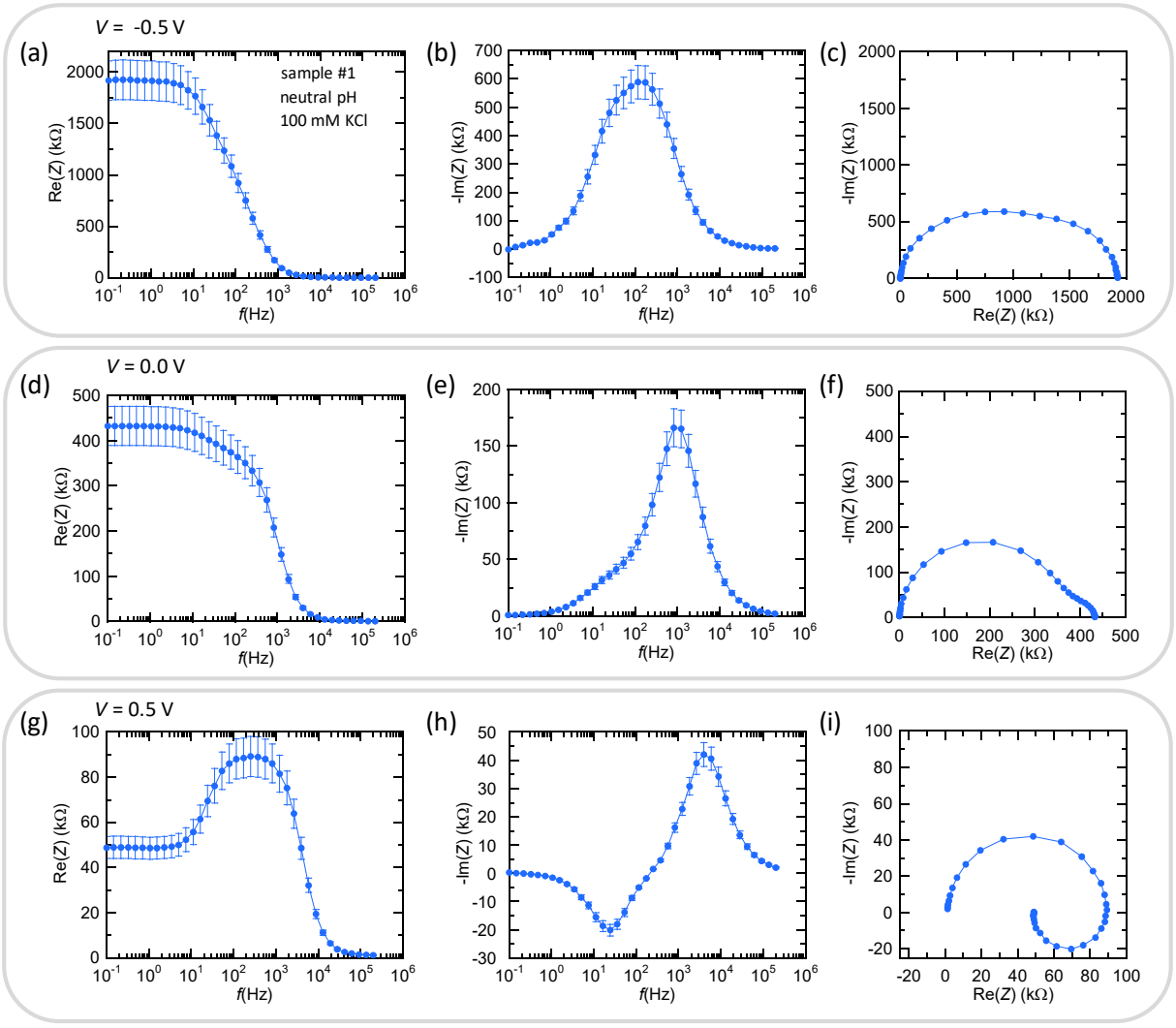

Fig. 2. The real Re(Z) *vs.* f, imaginary Im(Z) *vs.* f, and Im (Z) *vs.* Re(Z) (Nyquist) plots of the membrane (sample #1) in 100 mM KCl solutions at neutral pH and different signal amplitudes: (a) – (c) reverse polarization at –0.5 V; (d) – (f) the limit voltage 0 V; (g) – (i) forward polarization at 0.5 V. The experimental errors remained below 10% for the impedance spectra. Note that the uncertainties in the Nyquist plots have already given in the corresponding Re(Z) and Im(Z) vs. f curves.

Fig. 3 provides a theoretical explanation of the chemical inductance effects of Fig. 2. For the negatively charged pore obtained at neutral pH, the majority ions conducting the current are the cations while the minority ions are the anions. However, the anions can still be forced

towards the pore when the cations accumulate at the tip to preserve the local electroneutrality, as shown in Fig. 3. Thus, the majority and minority ion concentrations are coupled, as shown in Fig. 3a and 3b for the local average concentrations $\langle c_+ \rangle$ and $\langle c_- \rangle$, respectively. The two concentration profiles are obtained using a physical model based on the Nernst–Planck and Poisson equations described with detail in Ref. [25].

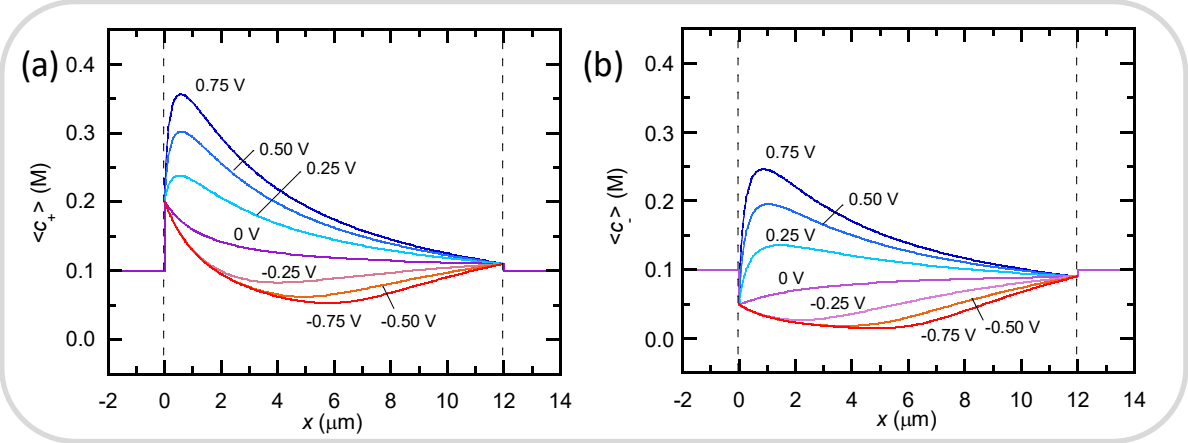

Fig. 3. (a) Local, steady state average concentrations of the majority (cations) mobile ions, as a function of the axial conical pore coordinate x, parametrically in the voltage V. (b) The local concentrations for the case of the minority (anions) mobile ions.

Because of its nanoscale dimensions, the pore tip dominates the ionic conduction. In this region, the surface density of the pore charges is high and thus the axial electric potential profile is strongly nonlinear [25]. For the forward polarization $V > 0$, the mobile ions accumulate at the tip following the cation entry to the pore; thus, the conductance is high (Fig. 3). On the contrary, for the reverse polarization $V < 0$, the ions are depleted at the tip because of the cation exit from the pore; thus, the conductance is low. The inductance effects observed in Figs. 2h and 2i arise from the high accumulation of mobile ions that has to be perturbed following the external signal changes, which occurs only at $V > 0$ (Fig. 3). Note that these ions interact strongly with the pore surface charges, which leads to hysteresis and memory effects

144 when the ionic solution at the pore tip cannot follow instantaneously the imposed changes in
145 the external voltage signal [27,28].

146 To show further the high tunability of the nanoporous membrane, Fig. 4 shows the $I - V$
147 curves obtained for a broad KCl concentration range (Fig. 4a), different salts LiCl, NaCl, and
148 KCl (Fig. 4b), monovalent and divalent cation salts (Fig. 4c), and solution pH values (Fig. 4d).
149 Fig. 4a shows that the current does not scale linearly with the ionic concentration because of
150 the dominant effects of the pore surface charges at low salt concentrations [25]. The currents
151 follow the ionic mobility series $Li^+ < Na^+ < K^+$ (Fig. 2b), suggesting the validity of general ionic
152 conduction principles [34,35]. Fig. 2c shows that the rectification effects tend to decrease for
153 divalent cations compared with monovalent cations because of the increased Debye screening
154 of the pore surface charges [34]. Note also the different rectifications obtained for distinct pH
155 values (Fig. 4d). We aim here at showing the effects associated with the conversion of a
156 negatively charged to a positively charged membrane at pH = 2, rather than keeping strictly
157 constant the ionic strength.

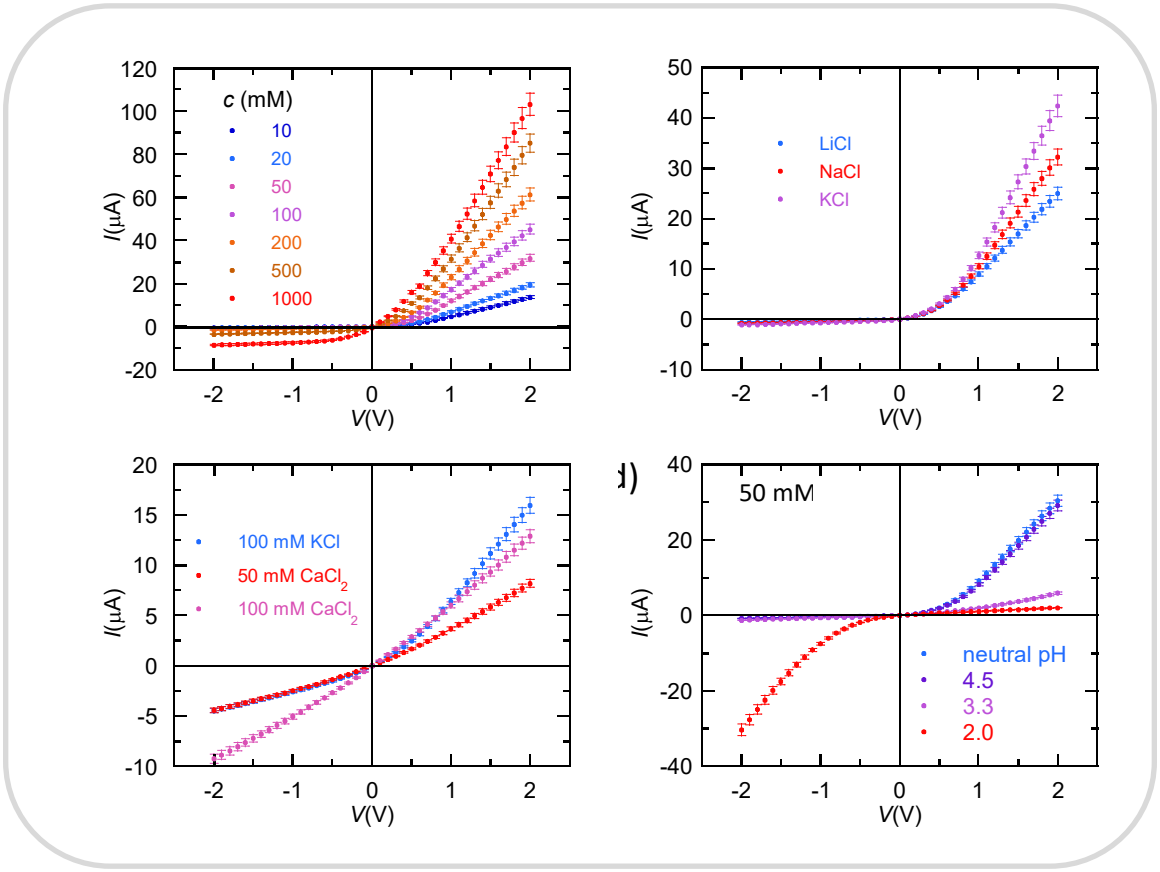

158

159 **Fig. 4.** The membrane $I - V$ curves for the cases: (a) different KCl concentrations in the range
160 $c = 10 - 1000$ mM at neutral pH (sample #1); (b) different salts LiCl, NaCl, and KCl at $c = 100$
161 mM at neutral pH (sample #1); (c) monovalent ($c = 100$ mM KCl) and divalent ($c = 50$ mM and
162 100 mM $CaCl_2$) cation salts at neutral pH (sample #2); (d) different pH values, from neutral pH
163 (negatively charged membrane pores) to pH = 2.0 (positively charged membrane pores) in
164 sample #1.

165

166 Fig. 5. shows the Re(Z) *vs.* f, Im(Z) *vs.* f, and Nyquist plots at different reverse and
167 forward polarization amplitudes. The impedances tend to approximately constant values at high
168 positive and negative voltages, as shown for the differential ratio dV/dI in Fig. 1d. Interestingly,
169 the inductance effects observed in Fig. 2 for the forward polarization case tend to disappear at
170 high positive voltages (Fig. 5f). The inductance effects observed in Figs. 2h and 2i were due to
171 the interaction of the mobile ions with the pore surface charges (Fig. 3). At high enough values

of V, however, the accumulation of mobile ions results in a high Debye screening of the pore surface charges. This fact decreases the above interaction and eventually eliminates the maximum of Re(Z) in Fig. 5d and the inductance effects in Fig. 5f, as shown by the fact that $-\mathrm{Im}(Z) > 0$ at high voltage V.

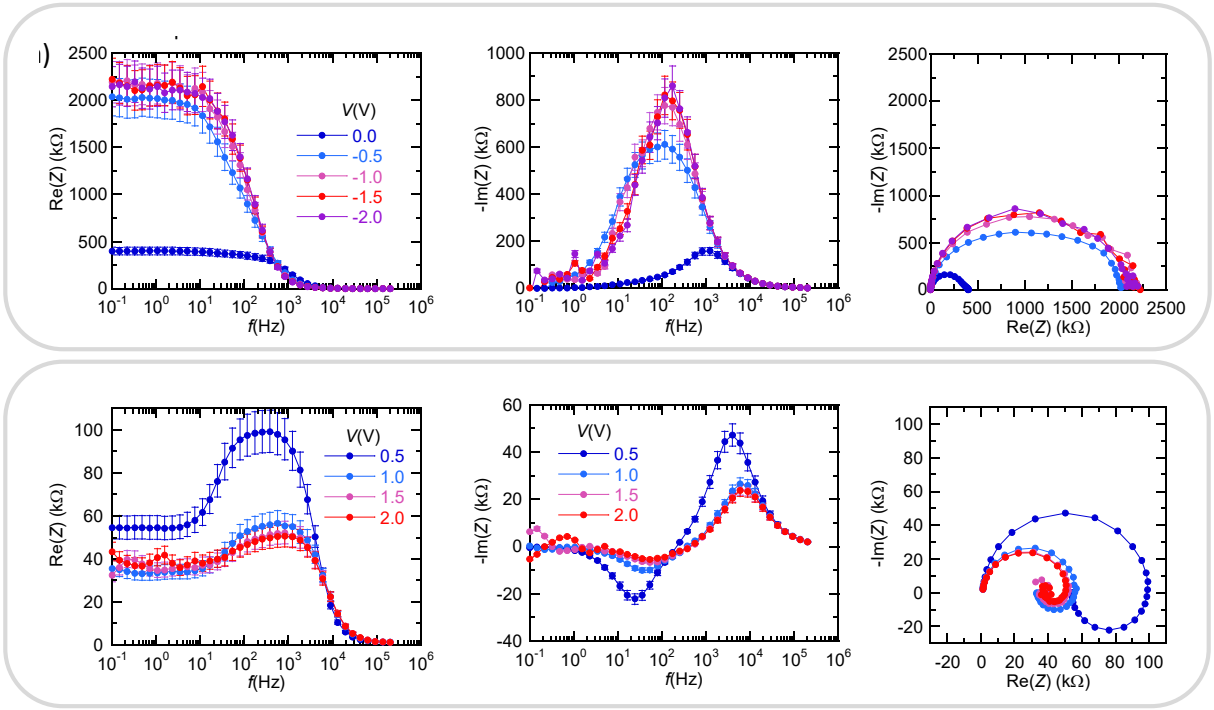

Fig. 5. Re(Z) *vs.* f, Im(Z) *vs.* f, and Nyquist plots of the membrane (sample #1) obtained in 100 mM KCl solutions at neutral pH and the signal amplitudes shown in the insets: (a) – (c) reverse polarization; (d) – (f) forward polarization.

Fig. 6 considers the effects of the salt concentration c on the impedance spectra for different membrane polarizations. As expected, Re(Z) decreases significantly with c reflecting the increase of the membrane conductance with the mobile ion concentrations (Fig. 2a). Also, Im(Z) decreases with c because of the increase in the effective membrane capacitance with the ionic solution concentration [36]. Note the dramatic decrease of the inductance effects with c

(Figs. 6h and 6i) due to the increase of the Debye screening with the ionic concentrations in the vicinity of the pore surface charges.

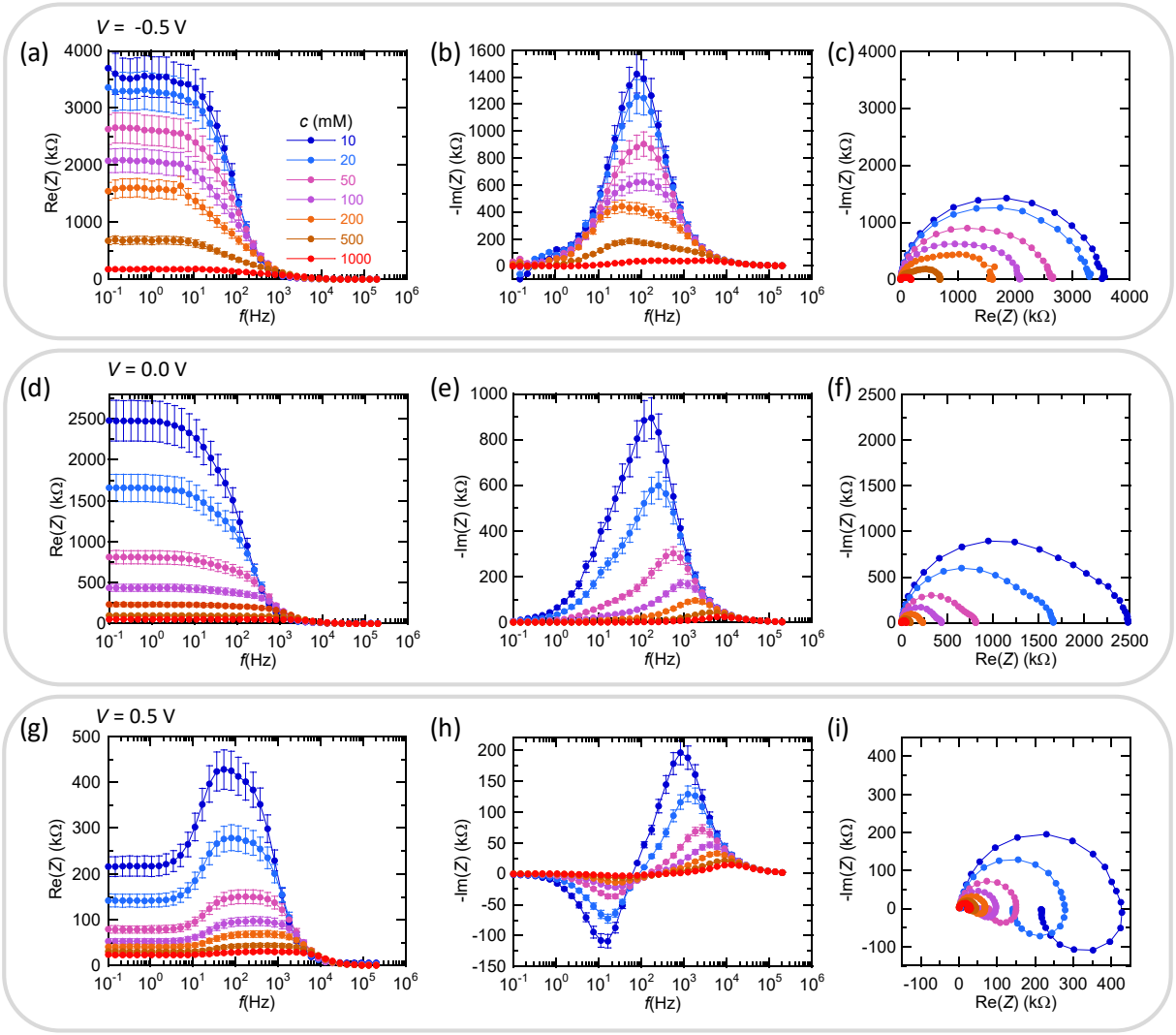

Fig. 6. Re(Z) *vs.* f, Im(Z) *vs.* f, and Nyquist plots of the membrane (sample #1) for different KCl concentration solutions at neutral pH: (a) – (c) reverse polarization at –0.5 V; (d) – (f) the limit voltage 0 V; (g) – (i) forward polarization at 0.5 V.

Fig. 7 analyzes the role of the solution pH on the impedance spectra for different polarizations. The pH effects are complex because of the multiple roles played by the water ions in the membrane. First, decreasing the solution pH from the neutral value causes a decrease in the ionization degree of the carboxylic groups functionalized on the pore surface [25,30].

This process decreases the absolute value of the negative pore charge density and weakens its effect on the ionic solution [25]. Second, a significant pH decrease may produce an additional effect: to provide high mobility hydrogen ions that eventually compete with the potassium ions for conduction. A third effect is also possible (Fig. 4d): at low enough pH, the effective pore charge groups can be positive rather than negative [30]. Note also the additional effect due to the membrane asymmetry and the sign of the voltage V: the hydrogen ions enter the pore tip for $V > 0$ while they exit the tip for $V < 0$ (Fig. 1b). Taken together, these competing effects results in a voltage-dependent behavior of the membrane impedance Z with the pH, as shown by Re(Z) and Im(Z) (Figs. 7a, 7b, 7d, and 7e), together with complex inductance effects (Figs. 7c and 7i).

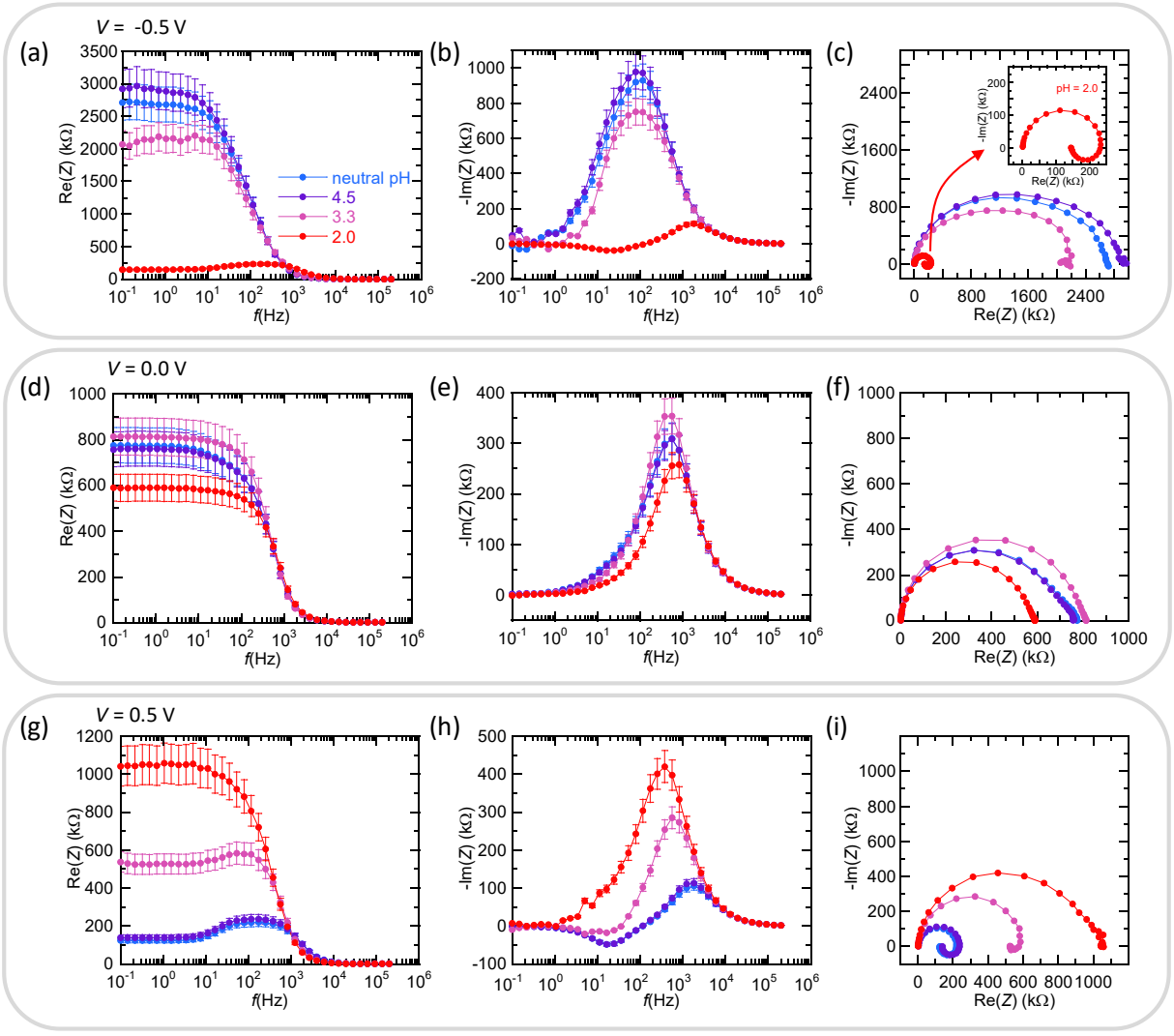

Fig. 7. Re(Z) *vs. f*, Im(Z) *vs. f*, and Nyquist plots of the membrane (sample #2) in 50 mM KCl solutions and the pH values shown in the insets: (a) – (c) reverse polarization at –0.5 V, (d) – (f) the limit voltage 0 V; (g) – (i) forward polarization at 0.5 V. The inset zooms the pH = 2 and V = –0.5 V case to better show the chemical inductance effects.

Membrane technology applications involve both monovalent and divalent cation salts. Figs. 8 and 9 consider the effects of different salts on the impedance spectra. Fig. 8 shows the case of the salt series LiCl, NaCl, and KCl while Fig. 9 compares the divalent cation salt $CaCl_2$ at different concentrations to the KCl salt. Note in particular the clear inductance effects observed for all monovalent cation salts (Figs. 8h and 8i) and the absence of these effects for the divalent cation salt (Figs. 9h and 9i) due to the high Debye screening of the negative pore charges caused by the Ca^{2+} ions.

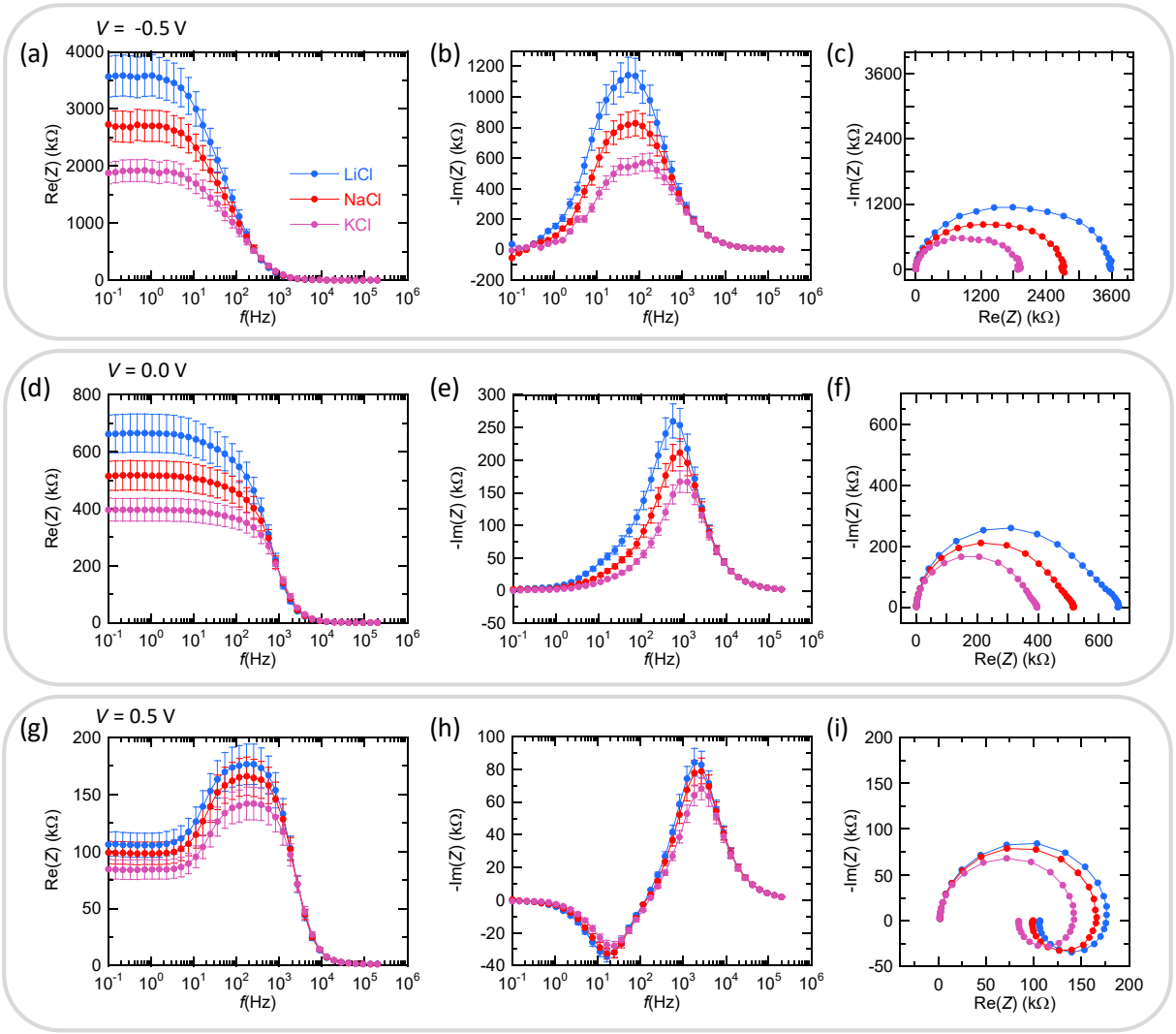

222

223 **Fig. 8.** Re(*Z*) *vs. f*, Im(*Z*) *vs. f*, and Nyquist plots of the membrane (sample #1) in 100 mM LiCl,

224 NaCl, and KCl solutions at neutral pH: (a) – (c) reverse polarization at –0.5 V; (d) – (f) the

225 limit voltage 0 V; (g) – (i) forward polarization at 0.5 V.

226

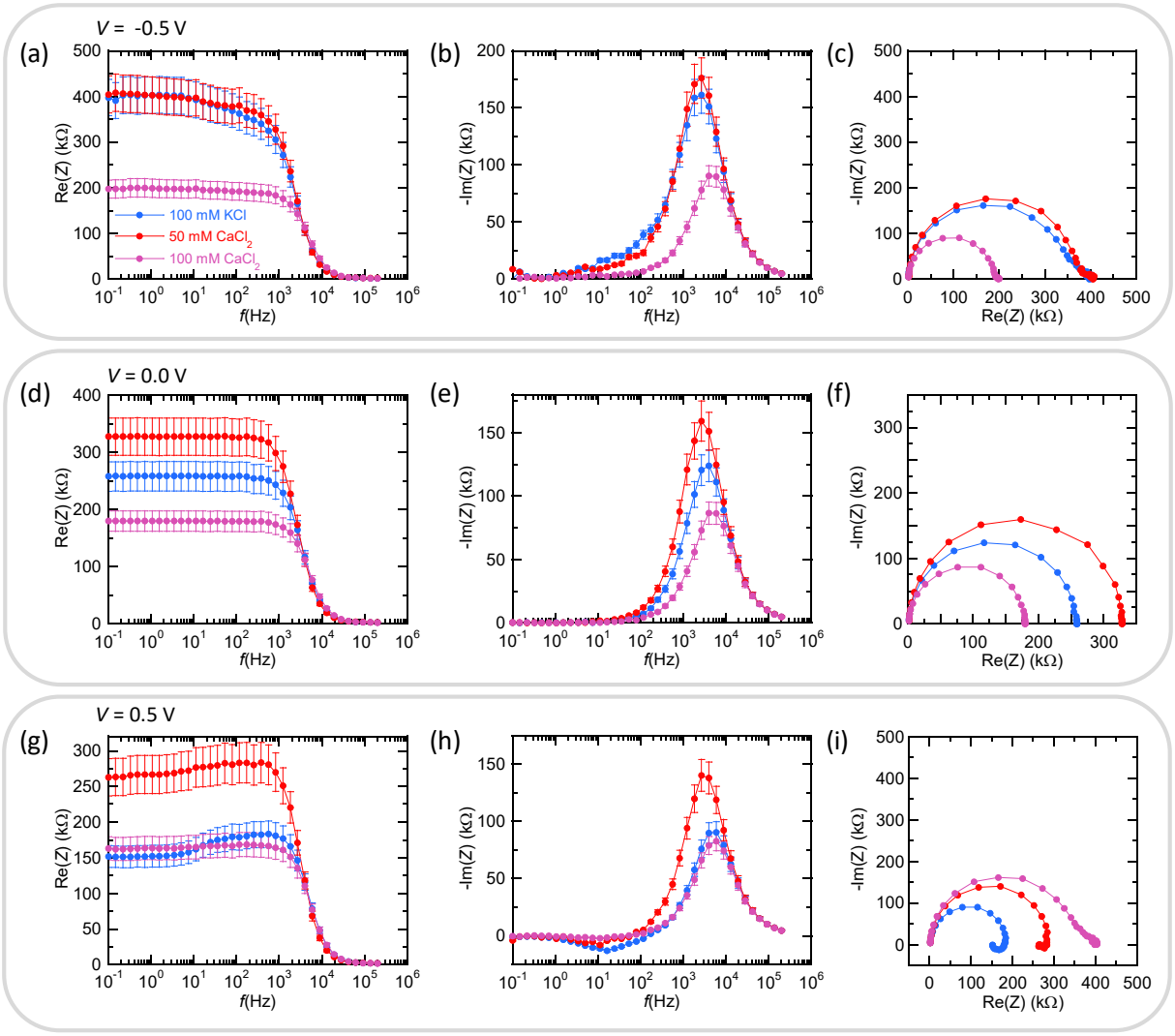

Fig. 9. Re(Z) *vs.* f, Im(Z) *vs.* f, and Nyquist plots of the membrane (sample #2) in a monovalent cation salt solution (100 mM KCl) and two divalent cation salt solutions (50 mM and 100 mM $CaCl_2$) at neutral pH: (a) – (c) reverse polarization at –0.5 V; (d) – (f) the limit voltage 0 V; (g) – (i) forward polarization at 0.5 V.

4. Conclusions

In summary, this work demonstrates that a multipore membrane with nanofluidic conical pores can be characterized by EIS techniques that allow to describe complex processes in the kinetic domain [4], [5], [6]. The different arcs observed in the impedance spectra allows to analyze the distinct physico-chemical phenomena occurring simultaneously in this complex

electrochemical system under operating conditions. In particular, we have described how the electrical interaction between the charges functionalized on the pore surface and those in the nanoconfined ionic solution changes with the amplitude and frequency of the external voltage signal, the electrolyte type and concentration, and the solution pH. Interestingly, new chemical inductance effects are observed that has not been discussed previously with these pores [29], [30].

The multipore membrane allowed robust responses by maximizing current output through an ensemble of pores [17] and des not demand exceedingly difficult operational procedures. Also, the scalability and biocompatibility of the pores suggested great potential for new hybrid biodevices and interfaces [17,21-23] and further work is now under way. In particular, the broad modulation of membrane conduction and electrical rectification, which is based on surface chemistry concepts, should be useful for implementing logic functions [37], iontronics circuitry [38,39], and chemically-gated transistors in membrane bioelectrochemistry [17,40].

CRediT authorship contribution statement

Patricio Ramirez: Conceptualization, Investigation, Data Curation, Methodology, Formal Analysis, Writing –Review & Editing. **Javier Cervera:** Formal Analysis, Project administration, Funding acquisition, Writing – Review & Editing. **Saima Nasir:** Investigation, Methodology, Formal Analysis. **Mubarak Ali:** Investigation, Methodology, Formal analysis, Writing – Review & Editing. **Wolfgang Ensinger:** Supervision, Project administration, Funding acquisition. **Salvador Mafe:** Formal analysis, Supervision, Project administration, Funding acquisition, Writing – Original Draft.

Declaration of Competing Interest

The authors declare that they have no known competing financial interests or personal relationships that could have appeared to influence the work reported in this paper.

Data availability

Data will be made available on request.

Acknowledgments

P.R., J.C., and S.M. acknowledge the support from the *Ministerio de Ciencia e Innovación* (Spain) and the *European Regional Development Funds* (FEDER), project No. PID2022-139953NB-I00, and the *Conselleria d'Educació, Universitats i Ocupació* (*Generalitat Valenciana*), project CIAICO2022-247. S.M. thanks UV for granting a sabbatical leave to UPV. M.A., S.N, and W.E. acknowledge the funding from the Hessen State Ministry of Higher Education, Research and the Arts, Germany, under the LOEWE project iNAPO.

References

[1] B. K. Shrestha, R. Ahmad, H. M. Mousa, I.-G. Kim, J. I. Kim, M. P. Neupane, C. H. Park, C. Sang Kim, High-performance glucose biosensor based on chitosan-glucose oxidase immobilized polypyrrole/Nafion/functionalized multi-walled carbon nanotubes bio-nanohybrid film, J. Colloid Interface Sci. 482 (2016) 39-47.

[2] N. Chen, S. Che, Y. Yuan, H. Liu, N. Ta, G. Li, F. J. Chen, G. Ma, B. Jiang, N. Wu, W. Yu, F. Yang, Y. Li, Self-supporting electrocatalyst constructed from in-situ transformation of Co(OH)2 to metal-organic framework to Co/CoP/NC nanosheets for high-current-density water splitting, J. Colloid Interface Sci. 645 (2023) 513-524.

[3] M. Algarra, A. L. Cuevas, M. V. Martínez de Yuso, J. Benavente, Insights into the formation of an emissive CdTe-quantum-dots/cellulose hybrid film, J. Colloid Interface Sci. 579 (2020) 714-722.

[4] N.D. Pismenskaya, O.A. Rybalkina, A.E. Kozmai, K.A. Tsygurina, E.D. Melnikova, V.V. Nikonenko, Generation of H^+ and OH^- ions in anion-exchange membrane/ampholyte-containing solution systems: A study using electrochemical impedance spectroscopy, J. Membrane Sci. 601 (2020) 117920.

[5] L. Zhang, H. Jia, J. Wang, H. Wen, J. Li, Characterization of fouling and concentration polarization in ion exchange membrane by in-situ electrochemical impedance spectroscopy, J. Membrane Sci. 594 (2020) 117443.

[6] A. Alcaraz, P. Ramırez J. A. Manzanares, S. Mafe, Conductive and Capacitive Properties of the Bipolar Membrane Junction Studied by AC Impedance Spectroscopy, J. Phys. Chem. B 105 (2001) 11669−11677.

[7] K. Kitta, M. Sakamoto, K. Hayakawa, A. Nukazuka, K. Kano, T. Yamamoto, Nanopore Impedance Spectroscopy Reveals Electrical Properties of Single Nanoparticles for Detecting and Identifying Pathogenic Viruses, ACS Omega 8 (2023) 14684−14693.

[8] K. Kant, J. Yu, C. Priest, J. G. Shaptera, D. Losic, Impedance nanopore biosensor: influence of pore dimensions on biosensing performance, Analyst 139 (2014) 1134−1140.

[9] Y. Lu, D. Zhang, Q. Zhang, Y. Huang, S. Luo, Y. Yao, S. Li, Q. Liu, Impedance spectroscopy analysis of human odorant binding proteins immobilized on nanopore arrays for biochemical detection, Biosens. Bioelectron. 79 (2016) 251–257.

[10] J. Feng, J. Liu, B. Wu, G. Wang, Impedance Characteristics of Amine Modified Single Glass Nanopores, Anal. Chem. 82 (2010) 4520–4528.

[11] A. Sokirko, P. Ramirez, J. A. Manzanares, S. Mafe, Modeling of forward and reverse bias conditions in bipolar membranes, Ber. Bunsenges. Phys. Chem. 97 (1993) 1040−1049.

[12] R. Fu, H. Wang, J. Yan, R. Li, C. Jiang, Y. Wang, T. Xu, Asymmetric bipolar membrane electrodialysis for acid and base production, AIChE J. 69 (2023) e17957.

[13] S. Bannwarth, M. Darestani, H. Coster, M. Wessling, Characterization of hollow fiber membranes by impedance spectroscopy, J. Membrane Sci. 473 (2015) 318−326.

[14] M.-C. Chien, G. J. Guang, M.-C. Yu, Nanopore Size Estimation by Electrochemical Impedance Spectroscopy Analysis, Jpn. J. Appl. Phys. 47 (2008) 7459−7463.

[15] M. J. Vitarelli, D. S. Talaga, Theoretical models for electrochemical impedance spectroscopy and local ζ-potential of unfolded proteins in nanopores, J. Chem. Phys. 139 (2013) 105101.

[16] J. Bisquert, Electrical Charge Coupling Dominates the Hysteresis Effect of Halide Perovskite Devices, J. Phys. Chem. Lett. 14 (2023) 1014−1021.

[17] Z. S. Siwy, M.L. Bruening, S. Howorka, Nanopores: synergy from DNA sequencing to industrial filtration – small holes with big impact, Chem. Soc. Rev. 52 (2023) 1983 – 1994.

[18] Y. Hou, Y. Ling, Y. Wang, M. Wang, Y. Chen, X. Li, X. Hou, Learning from the brain: bioinspired nanofluidics, J. Phys. Chem. Lett. 14 (2023) 2891 – 2900.
[19] M. Tagliazucchi, I. Szleifer, Transport mechanisms in nanopores and nanochannels: can we mimic nature?, Mater. Today 18 (2015) 131 – 142.
[20] K. Xiao, L. Wen, L. Jiang, Biomimetic solid-state nanochannels: From fundamental research to practical applications, Small 12 (2016) 2810 – 2831.
[21] G. Perez-Mitta, A.G. Albesa, C. Trautmann, M.E. Toimil-Molares, O. Azzaroni, Bioinspired integrated nanosystems based on solid-state nanopores: "iontronic" transduction of biological, chemical and physical stimuli, Chem. Sci. 8 (2017) 890 – 913.
[22] C. Li, T. Xiong, P. Yu, J. Fei, L. Mao, Synaptic Iontronic Devices for Brain-Mimicking Functions: Fundamentals and Applications, ACS Appl. Bio Mater. 4 (2021) 71−84.
[23] B. Xie, T. Xiong, W. Li, T. Gao, J. Zong, Y. Liu, P. Yu, Perspective on Nanofluidic Memristors: From Mechanism to Application, Chem. Asian J. 17 (2022) e202200682.
[24] A. Noy, S.B. Darling, Nanofluidic Computing Makes a Splash, Science 379 (2023) 143−144.
[25] J. Cervera, B. Schiedt, R. Neumann, S. Mafe, P. Ramirez, Ionic conduction, rectification, and selectivity in single conical nanopores, J. Chem. Phys. 124 (2006) 104706.
[26] I. Vlassiouk, Z.S. Siwy, Nanofluidic Diode, Nano Lett. 7 (2007) 552−556.
[27] D. Wang, M. Kvetny, J. Liu, W. Brown, Y. Li, G. Wang, Transmembrane Potential across Single Conical Nanopores and Resulting Memristive and Memcapacitive Ion Transport, J. Am. Chem. Soc. 134 (2012) 3651−3654.
[28] D. Wang, W. Brown, Y. Li, M. Kvetny, J. Liu, G. Wang, Hysteresis Charges in the Dynamic Enrichment and Depletion of Ions in Single Conical Nanopores, ChemElectroChem. 5 (2018) 3089−3095.
[29] J. Cervera, P. Ramirez, S. Nasir, M. Ali, W. Ensinger, Z.S. Siwy, S. Mafe, Cation pumping against a concentration gradient in conical nanopores characterized by load capacitors. Bioelectrochem. 152 (2023)108445.
[30] P. Ramirez, V. Garcia-Morales, V. Gomez, M. Ali, S. Nasir, W. Ensinger, S. Mafe, Hybrid circuits with nanofluidic diodes and load capacitors, Phys. Rev. Applied 7 (2017) 064035.
[31] P. Apel, Track etching technique in membrane technology, Radiat. Meas. 34 (2001) 559 – 566.
[32] Z. Siwy, D. Dobrev, R. Neumann, C. Trautmann, K. Voss, Electro-responsive asymmetric nanopores in polyimide with stable ion-current signal, Appl. Phys. A 76 (2003) 781 – 785.
[33] J. Bisquert, A. Guerrero, Chemical Inductor, J. Am. Chem. Soc. 144 (2022) 5996−6009.
[34] P. Ramirez, J.A. Manzanares, J. Cervera, V. Gomez, M. Ali, I. Pause, W. Ensinger, S. Mafe, Nanopore charge inversion and current-voltage curves in mixtures of asymmetric electrolytes, J. Membrane Sci. 563 (2018) 633–642.
[35] J. J. Perez-Grau, J. Cervera, S. Nasir, M. Ali, W. Ensinger, P. Ramirez, S. Mafe, Additivity of ionic currents in mixed electrolyte solutions and confined geometries, J. Mol. Liq. 360 (2022) 119592.
[36] M. Tajparast, M. I. Glavinović, Effect of ion concentration, solution and membrane permittivity on electric energy storage and capacitance, Biochim. Biophys. Acta-Biomembranes 1860 (2018) 2385–2403.
[37] V. Gomez, P. Ramirez, J. Cervera, M. Ali, S. Nasir, W. Ensinger, S. Mafe, Concatenated logic functions using nanofluidic diodes with all-electrical inputs and outputs. Electrochem. Commun. 88 (2018) 52 – 56.
[38] M. Ali, P. Ramirez, S. Nasir, J. Cervera, S. Mafe, W. Ensinger, Ionic circuitry with nanofluidic diodes, Soft Matter 15 (2019) 9682 – 9689.
[39] P. Ramirez, J. Cervera, V. Gomez, M. Ali, S. Nasir, W. Ensinger, S. Mafe, Modulation of current-time traces by twopore arrangements of polyimide nanofluidic diodes, Appl. Phys. Lett. 115 (2019) 183701.

373 [40] P. Ramirez, M. Ali, W. Ensinger, and S. Mafe, Appl. Phys. Lett. 101 (2012) 133108.
374
375

376 Graphical Abstract

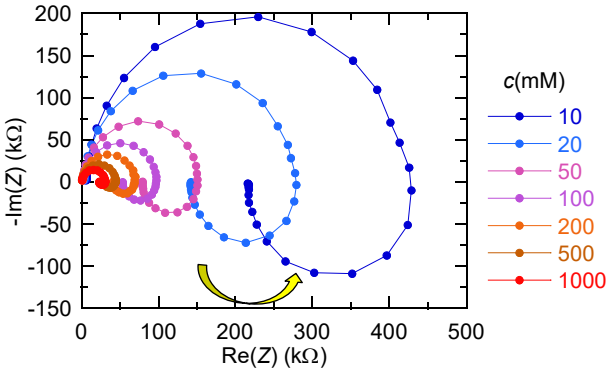

377